Experimental Hematology

Experimental Hematology 2021;97:57–65

REGULAR SUBMISSION

The delta isoform of phosphatidylinositol-3-kinase predominates in chronic myelomonocytic leukemia and can be targeted effectively with umbralisib and ruxolitinib

Matthew T. Villaume[a,b], M. Pia Arrate[a], Haley E. Ramsey[a,b], Kathryn I. Sunthankar[a], Matthew T. Jenkins[a,c], Tamara K. Moyo[a], Brianna N. Smith[b,d], Melissa A. Fischer[a,b], Merrida A. Childress[a,b], Agnieszka E. Gorska[a], P. Brent Ferrell[a,b,e,f], and Michael R. Savona[a,b,e,f]

[a]*Department of Medicine, Vanderbilt University School of Medicine, Nashville, TN;* [b]*Program in Cancer Biology, Vanderbilt University School of Medicine, Nashville, TN;* [c]*Department of Pharmacology, Vanderbilt University School of Medicine, Nashville, TN;* [d]*Department of Pediatrics, Vanderbilt University School of Medicine, Nashville, TN;* [e]*Center for Immunobiology, Vanderbilt University School of Medicine, Nashville, TN;* [f]*Vanderbilt–Ingram Cancer Center, Vanderbilt University School of Medicine, Nashville, TN*

(Received 11 July 2020; revised 11 February 2021; accepted 12 February 2021)

Chronic myelomonocytic leukemia (CMML) is a myelodysplastic syndrome/myeloproliferative neoplasm overlap syndrome characterized by monocytic proliferation in the presence of dysplastic bone marrow changes, inflammatory symptoms, and propensity for transformation to acute myeloid leukemia (AML), with a poor prognosis and limited treatment options. Unlike the α and β isoforms, the phosphatidylinositol-3-kinase (PI3K)−δ signaling protein is predominantly expressed by hematopoietic cells and therefore has garnered interest as a potential target for the treatment of lymphomas and leukemias. We revealed a pattern of increased PIK3CD:PIK3CA ratio in monocytic M5 AML patients and cell lines, and this ratio correlated with responsiveness to pharmacological PI3K-δ inhibition in vitro. Because CMML is a disease defined by monocytic clonal proliferation, we tested the PI3K-δ inhibitor umbralisib as a single agent and in combination with the JAK1/2 inhibitor ruxolitinib, in CMML. Our ex vivo experiments with primary CMML patient samples revealed synergistic inhibition of viability and clonogenicity with this combination. Phospho-specific flow cytometry revealed that dual inhibition had the unique ability to decrease STAT5, ERK, AKT, and S6 phosphorylation simultaneously, which offers a mechanistic hypothesis for the enhanced efficacy of the combination treatment. These preclinical data indicate promising activity by co-inhibition of PI3K-δ and JAK1/2 and support the use of ruxolitinib + umbralisib combination therapy in CMML under active clinical investigation. © 2021 Published by Elsevier Inc. on behalf of ISEH – Society for Hematology and Stem Cells.

Chronic myelomonocytic leukemia (CMML) is a myelodysplastic syndrome/myeloproliferative neoplasm overlap syndrome (MDS/MPN) characterized by monocytic proliferation in the presence of other cytopenias, splenomegaly, and propensity for transformation to acute myeloid leukemia (AML). Prognosis is generally poor, with a mean overall survival between 2 and 5 years [1]. Response to conventional treatment is variable, and the only curative treatment is allogeneic hematopoietic stem cell transplantation (HSCT). Preclinical observations of hypersensitivity to janus kinase/signal transducer and

MTV, MPA, KIS, MTJ, PBF, and MRS designed or performed experiments. MTV, KIS, HER, BNS, MAF, AEG, and MRS analyzed data. MTV, MTJ, and MRS performed statistical analysis and wrote the article. PBF and MRS supervised the study. All authors reviewed and edited drafts of the article and approved the final version of the article.

Supplementary data related to this article can be found online at https://doi.org/10.1016/j.exphem.2021.02.008

Offprint requests to: Michael R. Savona, Vanderbilt University School of Medicine, 777 Preston Research Building, 2220 Pierce Avenue, Nashville, TN 37232; E-mail: michael.savona@vanderbilt.edu

Supplementary material associated with this article can be found in the online version at https://doi.org/10.1016/j.exphem.2021.02.008.

0301-472X/© 2021 Published by Elsevier Inc. on behalf of ISEH – Society for Hematology and Stem Cells.
https://doi.org/10.1016/j.exphem.2021.02.008

activator of transcription (JAK/STAT)-dependent granulocyte–macrophage colony-stimulating factor (GM-CSF) signaling in CMML have led to successful trials testing JAK inhibitors in the clinic [2–4]. Compensatory JAK2/STAT5 signaling following phosphatidylinositol-3-kinase (PI3K)/AKT inhibition has been observed in breast cancer models, spurring interest in inhibiting both signaling pathways simultaneously [5]. Co-targeting of the JAK/STAT and PI3K/AKT pathways has been investigated preclinically in a range of neoplasms, with promising results, including in myleofibrosis [6,7]. Considerable pharmaceutical efforts toward inhibiting the PI3K/AKT pathway have focused on inhibitors that are specific to one or more of the four class I PI3K catalytic subunit isoforms (p110-α,β,δ,γ), and strong in vitro growth inhibitory synergy between a PI3K-δ-specific inhibitor and a JAK1/2 inhibitor has been previously reported in myeloid leukemia patient samples, including a single CMML patient sample [8].

Umbralisib (TGR-1202) is a PI3K-δ isoform-selective and casein kinase 1-ε (CK1ε) inhibitor that has had impressive responses in clinical trials for the treatment of lymphoid malignancies, which are known to be reliant on the PI3K-δ subunit for AKT activation and survival [9]. Unlike the ubiquitously expressed PI3K-α and $-\beta$ isoforms, PI3K-δ is confined largely to hematopoietic cells, and has been identified as the predominant isoform seen in bone marrow aspirates from AML patients, although its role in CMML has yet to be investigated [10,11]. An ongoing clinical trial in a related myeloid disease, myelofibrosis, reported that umbralisib augmented the response to ruxolitinib in patients previously resistant to ruxolitinib monotherapy, and resulted in a complete response (CR) in 2 patients (International Working Group—Myeloproliferative Neoplasms Research and Treatment (IWG-MRT) consensus criteria, response rate = 56.5%) [12]. Here, we evaluated the efficacy of umbralisib in combination with ruxolitinib in human leukemia cell lines and primary CMML patient samples to provide support for this combination as a new therapeutic strategy in CMML.

Methods

Patient samples

Experiments were conducted on viably frozen, primary CMML patient samples, which were provided by the Vanderbilt–-=Ingram Cancer Center Hematologic Malignancy Tumor Bank in accordance with the tenets of the Declaration of Helsinki and approved by the Vanderbilt University Medical Center Institutional Review Board.

Cell lines

AML cell lines MV-4-11, Kasumi-1, K-562, U-937, Kasumi-3, PL-21, MOLM-16, and THP-1 and leukemia mantle cell lymphoma cell line Z-138 were purchased from the American Type Culture Collection (ATCC, Manassas, VA). OCI-AML3, HEL, F36P, and MOLM-13 cell lines were purchased from Deutsche Sammlung von Mikroorganismen und Zellkulturen (DSMZ, Braunschweig, Germany). ATCC and DSMZ cell bank cell lines were authenticated by short tandem repeat profiling and cytochrome c oxidase gene analysis. Cultured cells were split every 3 to 4 days and maintained in exponential growth phase. Cell lines were tested for *Mycoplasma* in 2019 using the Universal Mycoplasma Detection Kit (ATCC). Cells were used for the experiments presented here within 10 to 30 passages from thawing. The MV-4-11 cell line was grown in Iscove's modified Dulbecco's medium (IMDM), the THP-1 cell line was grown in RPMI-1640 supplemented with 10% fetal bovine serum (FBS) and 0.05 mmol/L 2-mercaptoethanol, and all other cell lines were cultured in RPMI-1640 and supplemented with 10% to 20% FBS. Cells were kept at 37°C in a 5% CO_2 incubator. All media were supplemented with 100 U/mL penicillin and 100 μg/mL streptomycin.

Protein extracts and Western blotting analysis

Cell lines were grown in their respective media before total protein lysates were extracted in Laemmli sample buffer (Bio-Rad, Hercules, CA), sonicated, and boiled at 95°C for 10 min. The samples were loaded in a 10% sodium dodecyl sulfate–polyacrylamide gel (3.6 μg protein/well for patient samples and 1.67×10^5 cells/well for cell lines). Cryopreserved CMML patient samples were resuspended in RPMI-1640 supplemented with 10% FBS and immediately exposed to RIPA lysis buffer; then lysates were extracted with RIPA extraction buffer and boiled at 95°C for 10 min. Western blot analysis was performed according to standard protocol with antibodies to PI3K-α (C73F8 clone, Cell Signaling Technology), PI3K-β (C33D4 clone, Cell Signaling Technology, Danvers, MA), Pi3k-δ (D1Q7R clone, Cell Signaling Technology), PI3K-γ (D55D5 clone, Cell Signaling Technology), and actin (Sigma-Aldrich, St. Louis, MO). The relative density of bands was measured using Li-COR (Lincoln, NE) Image Studio Lite version 5.2.

Gene expression data sets

Cell line AML subtype gene expression data were analyzed from microarray data ($\log_2$ expression) from the Hemap data set (http://hemap.uta.fi/) [13]. The data were generated using RNA extracted from the mononuclear cell fraction of AML patients. For healthy monocytes, only gene expression data from experimental controls not manipulated with drugs or cytokines were used. Cell line microarray data were gathered from the Cancer Cell Line Encyclopedia (CCLE), whose creators bear no responsibility for our analysis or interpretation [14]. For analysis of CMML gene expression, $\log_2$-transformed expression values of Affymetrix Human Genome U133 Plus 2.0 Array probe sets were downloaded from GEO (GSE42731, GSE61804). Heatmaps were generated using the Heatmapper resource (http://heatmapper.ca/expression/) using median $\log_2$ gene expression values from the Hemap data set [15]. Color shading represents the relative abundance of gene expression across each sample type, represented as the Z score.

In vitro growth inhibition assays

Cryopreserved CMML bone marrow (BM) mononuclear cells (MNCs) were resuspended in STEMSPAN serum-free expansion medium supplemented with 10 ng/mL GM-CSF (PeproTech, Rocky Hill, NJ). To determine the efficacy of umbralisib independently and in combination with ruxolitinib, cell lines or patient samples were plated into a 384-well plate and treated for 72 hours at 37°C and 5% CO_2 with umbralisib (provided by TG Therapeutics, New York, NY) or ruxolitinib (Selleckchem, Houston, TX) at concentrations ranging from 3 nmol/L to 10 μmol/L. Cell viability was measured using CellTiter-Glo reagent (Promega Corp, Madison, WI), and relative luminescence units (RLU) were measured with a microplate reader (BioTek, Winooski, VT). Viability was defined as the percentage of RLU of each well compared with the RLU of cells treated with a dimethyl sulfoxide (DMSO) vehicle. Data are expressed as the mean ± SD from three replicates for cell line experiments and two replicates in the case of patient samples.

Drug combination analysis and calculation of synergy

The effects of the combinations were calculated using the Zero Interaction Potency (ZIP) model, which compares observed and expected combination effects [16]. A detailed description and interpretation guide are included in the Supplementary Data (online only, available at www.exphem.org).

Colony formation assays

CMML bone marrow mononuclear cells (BMMCs) were resuspended as above and added to 3 mL of MethoCult H4230 methylcellulose (STEMCELL Technologies, Vancouver, BC, Canada) to a final concentration of $1-3 \times 10^5$ cells/mL containing GM-CSF (10 ng/mL) and either DMSO, 30 nmol/L ruxolitinib, 3.3 μmol/L umbralisib, or the combination. Next, 1.1 mL of the MethoCult solution was plated into 35 × 10-mm Petri dishes, in duplicate. Plates were incubated for 14 days at 37°C and 5% CO_2, and colony (defined as a cluster of >50 cells) counts were then determined under a microscope at 10 × magnification.

Flow cytometry

CMML BMMCs were resuspended as described above. Cells were treated with DMSO (<0.1% by volume), 100 nmol/L ruxolitinib, 10 μmol/L umbralisib, or their combination for 24 or 48 hours in an incubator at 37°C and 5% CO_2. $CD33^+CD45^+$ subpopulation measurements were taken at the 24-hour time point, whereas $CD34^+CD38^-$ viability is reported from the 48-hour time point measured in separate experiments. This was done to preserve adequate cell counts in the $CD33^+CD45^+$ population, which decreased in number more rapidly than the $CD34^+CD38^-$ population. Cells were stained with a combination of antibodies against human CD33-PE/Cy7 (Clone P67.6, BioLegend, San Diego, CA), CD45-APC (Clone 2D1, BioLegend), CD34-PE-Dazzle 594 (Clone 581, BioLegend), CD38-APC/Cy7 (Clone 90, BioLegend), and the AnnexinV/DAPI Apoptosis Detection Kit (BD Pharmingen, San Diego, CA) and subjected to flow-cytometric analysis using a four-laser LSR Fortessa (Becton Dickinson, Franklin Lakes, NJ).

Phospho-specific flow cytometry

Phospho-specific flow cytometry with fluorescence cell barcoding was performed as has previously been reported [17]. Briefly, cells (either patient samples or cell lines) were plated at 1×10^6 cells/mL and incubated with either DMSO, umbralisib (No. S8194, Selleck Chemicals, Houston, TX; 20 μmol/L), ruxolitinib (No. S1378, Selleck Chemicals; 60 nmol/L), or the combination for 30 min. Cells in the stimulated condition were subsequently stimulated with 20 ng/mL GM-CSF (No. 300-03-20UG, PeproTech) for 15 min, and all were then exposed to 50 × Ax700 (No. A20010, Invitrogen, Carlsbad, CA) viability stain. Cells were fixed in 1.6% paraformaldehyde (PFA, No. 50-980-487, Fisher Scientific, Waltham, MA) in the dark at room temperature for 10 min, washed with phosphate-buffered saline (PBS), permeabilized with MeOH (No. A4121, Fisher Scientific), and stored at −80°C. Cells were washed twice with PBS before barcoding with serial dilutions of Pacific Orange (1:2.5; No. P30253, Invitrogen) and Pacific Blue (1:2.4; No. P10163, Invitrogen) dyes and combining in a single tube [18,19]. Cells were stained with pSTAT5-PE/Cy7 (Clone 47, BD:560117), pERK-Ax488 (Clone 6B8B69, BioLegend No. 369508), pAKT-Ax488 (Clone M89-61, Becton-Dickinson No. 560404, and Clone D9E, Cell Signaling Technology No. 5315S), and pS6-Ax647 (Clone D57.2.2E, Cell Signaling Technology No. 4851S) in the dark at room temperature for 30 min. Cells were washed with 1 mL PBS/BSA, resuspended in 0.2 mL PBS/BSA, and analyzed with a four-laser LSR Fortessa.

Next-generation sequencing

For next-generation sequencing (NGS), CMML patient bone marrow aspirates were obtained, and DNA was isolated using a DNA Midi Kit (Qiagen, Hilden, Germany) for NGS in a panel of commonly mutated regions of myeloid neoplasia-associated genes across the genome. The analytic targets included in the OnkoSight NGS Myeloid Malignancies gene panel (Illumina, San Diego, CA) include exonic regions across each of the following genes: *SRSF,* U2*AF1, TET2, IDH2, DNMT3A, RUNX1,* TP5*3, BCOR, BCORL1, ETV6, NPM1, GATA2,* WT1*, ASXL1, EZH2, JAK2, FLT3, FBXW7, CBL, KRAS, NRAS, SETBP1, ABL1, CSF3R, PTEN, PTPN11, SRSF2,* TP5*3, ZRSR2, PHF6, MYD88, IDH1, HRAS, CALR, BRAF*, and *CDKN2A*. The panel of validated genes consisted of therapeutic markers, as well as genes with diagnostic and prognostic utility in myeloid and other hematologic tumors.

Statistical analysis

Statistical comparison of gene expression levels between myeloid leukemia subtypes was done using a two-tailed Wilcoxon test followed by Benjamini–Hochberg adjustment of p values, and fold change was computed to compare gene expression levels for *PIK3CA, PIK3CB, PIK3CD,* and *PIK3CG* using the National Institutes of Health's GEO2R Web-based tool (https://www.ncbi.nlm.nih.gov/geo/geo2r/). For the in vitro growth inhibition assays and the flow cytometry analysis of viability, differences in viability relative to

control between the treated groups were analyzed with a paired *t* test using GraphPad software analysis (Prism 6.0h; GraphPad, San Diego, CA). Dose–response curves were generated with GraphPad Prism version 6.0h, and 50% growth inhibition concentration (GI50) values were determined using linear regression of double-log transformed data. For comparison of colony-forming ability among treatment arms, a multiple regression analysis was performed comparing the relative viability of each single agent and the combination across the seven samples tested using Stata (Version 14).

Results

We first sought to assess the expression pattern of the PI3K isoforms in leukemic cell lines (Figure 1A). There were a range of expression levels across the 12 myeloid leukemia cell lines and 1 mantle cell lymphoma cell line tested for all four PI3K subunit isoforms. The PI3K-δ protein was most abundant in myelomonocytic and monocytic AML cell lines, histologically defined with the French–American–British (FAB) classification as M4 or M5. There was less expression in both erythroid leukemias (M6) and primitive leukemia cell lines (M0–M2 and the chronic myeloid leukemia [CML] blast crisis line K562). There were notable exceptions to this pattern of protein expression; however, the gene expression data generated a more consistent picture. Comparing publicly available microarray data sets from these cell lines revealed, again, a common pattern of decreased *PIK3CA* and increased *PIK3CD* in cell lines derived from M5 AML patients (Figure 1B) [14]—an unsurprising result given that PI3K-δ has been previously reported to be predominately regulated at the level of transcription [20].

This pattern also held true for gene expression data from primary human AML blasts, with M5 AMLs expressing more *PIK3CD* and less *PIK3CA* than other AML subtypes, including in isolated M5 $CD34^+$ hematopoietic progenitor cells (Figure 1C). We next analyzed a pair of data sets containing both CMML and AML patient samples and found an increase in *PIK3CD* expression in CMML compared with AML samples, though PIK3CA was equivalent in this case (Supplementary Figure E1 and Table E1, online only, available at www.exphem.org). The differences of both genes across disease types are best visualized by the *PIK3CD:PIK3CA* ratio, with M5 AML and CMML having the greatest ratio of delta to alpha (Figure 1D), but a statistical comparison of individual gene mean log fold differences across leukemia subtypes was also performed and was consistent with this representation (Supplementary Figure E1 and Table E1). The ratio of *PIK3CD* to *PIK3CA* gene expression has previously been reported to be correlated with response to PI3K-δ subunit inhibition in the clinic [22]. No other AML subtypes, nor other myeloid malignancies such as MDS and chronic myeloid leukemia (CML) followed this pattern of PI3K isoform gene expression (Supplementary Table E2, online only, available at www.exphem.org).

We next assessed the efficacy of umbralisib against select cell lines with varying PI3K-δ protein levels.

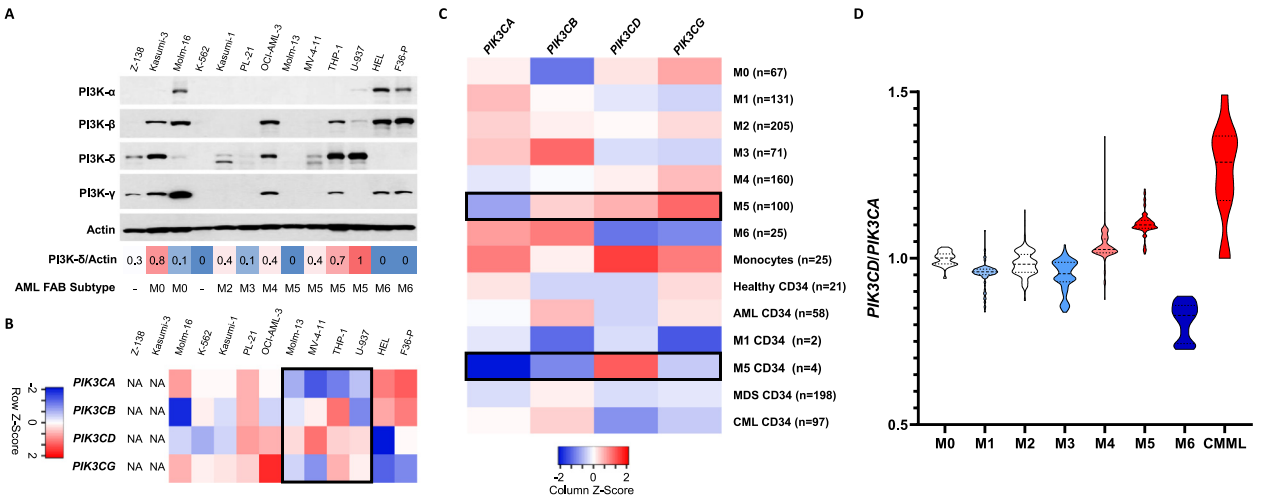

Figure 1. PI3K catalytic subunit expression patterns in myeloid leukemias. **(A)** Western blot analysis of 11 myeloid and 1 lymphoid neoplasm cell lines to determine protein levels of PI3K-δ. Actin was used as a loading control. The PI3K-δ/actin ratio describes the relative density of the Western blot band as measured with Image Studio Lite version 5.2. French–American–British (FAB) subtyping differentiates AML by cell maturity and origin based on histological evaluation. **(B)** Heatmap of the microarray median gene expression of PI3K catalytic subunit genes in available cell lines in the CCLE. **(C)** Heatmap of the median gene expression for each AML FAB class, healthy samples, healthy monocytes, and CD34+ cells from AML, MDS, CML, and healthy donor samples in the Hemap data set. **(D)** Violin plot of *PIK3CD* to *PIK3CA* median $\log_2$ gene expression ratio by AML FAB subtype from the Hemap data set. CMML data were gathered from Gelsi-Boyer et al. [21]. *NA*=not available.

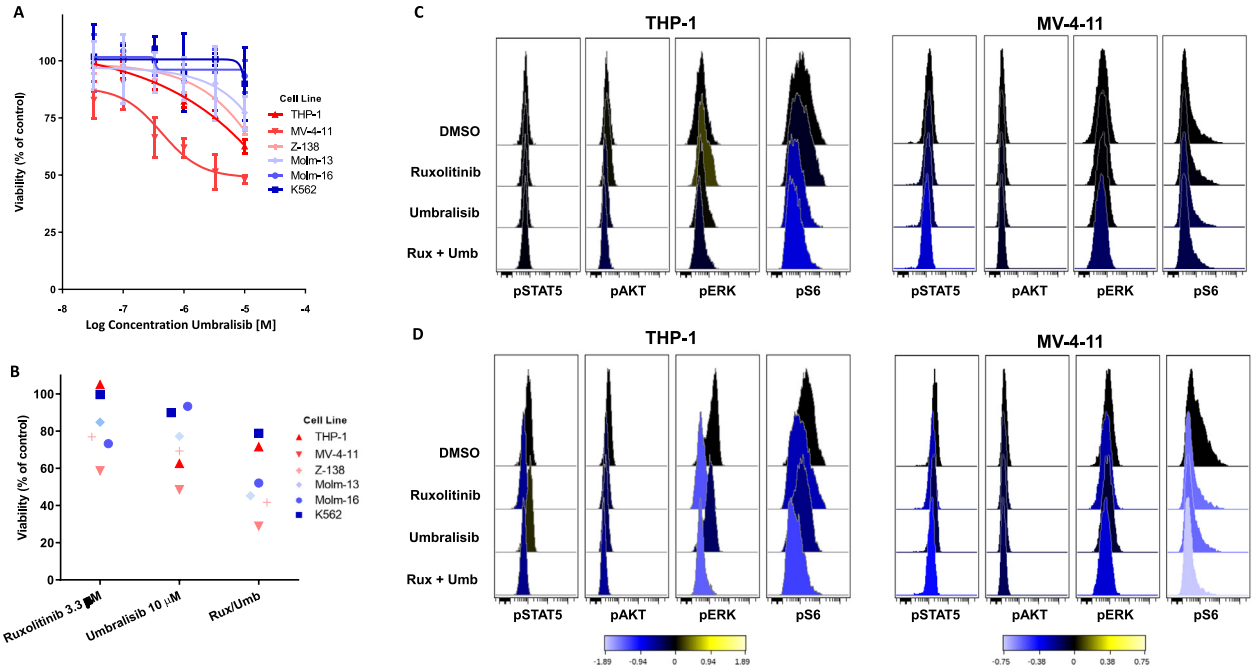

Figure 2. Ruxolitinib/umbralisib combination treatment of leukemia cell lines. **(A,B)** The viability of treated cell lines compared with the DMSO control using the CellTiter-Glo assay was plotted for **(A)** the indicated concentration gradient of solo agent umbralisib and **(B)** selected concentrations of ruxolitinib, umbralisib, and the combination. Each symbol represents the mean of three experimental replicates. The color associated with each cell line relates to the relative expression of PI3K-δ as determined by Western blot analysis. **(C,D)** Histograms from a representative experimental replicate ($n = 2$) of phospho-specific flow cytometry analysis of cell signaling responses of THP-1 and MV-4-11 cell lines to the combination treatment in the absence **(C)** and presence **(D)** of GM-CSF stimulation. Values represent the arcsinh of the median fold change from DMSO-treated cells.

Myeloid leukemia cell lines were largely insensitive to umbralisib as a solo agent, similar to the observed activity of the related compound, idelalisib, in AML samples (Figure 2A) [11]. However, a trend emerged wherein cell lines with increased PI3K-δ expression (THP-1, MV-4-11, Z-138) had the greatest dose response to umbralisib. The myelomonocytic (B-myeloid) leukemia cell line, MV-4-11, was the most sensitive with 50% growth inhibition (GI_{50}) reached at 5.7 μmol/L, and is also the only cell line tested where the PI3K-δ protein was the only isoform detected by Western blot. The combination of 3.3 μmol/L ruxolitinib and 10 μmol/L umbralisib, our highest doses tested, exhibited moderate ability to reduce growth across the cell lines, with MV-4-11 having the greatest growth inhibition in all three conditions. Umbralisib offered modest additive growth inhibition to ruxolitinib in cases where it had almost no activity as a solo agent, such as with Molm-16 and K-562 (Figure 1B). Interestingly, THP-1 was completely insensitive to ruxolitinib as a solo agent, in stark contrast to MV-4-11, the other PI3K-δ-predominant myeloid leukemia cell line tested.

To investigate this further, we examined cell signaling changes in both THP-1 and MV-4-11 in their typical cell culture conditions as described above, without the addition of cytokines (Figure 2C). As expected, umbralisib decreased pAKT and pS6 signaling in THP-1 cells. Interestingly, there was a paradoxical increase in pERK signaling when THP-1 cells were exposed to ruxolitinib alone, a pattern that was reversed when ruxolitinib was combined with umbralisib. MV-4-11 signaling changes were comparable to THP-1 with the solo agents; however, the combination exhibited a unique ability to decrease all four cell signaling molecules including pSTAT5. Because of our interest in CMML and its known hypersensitivity to GM-CSF stimulation, we also investigated in vitro cell signaling responses in the presence of this cytokine (Figure 2D). In both cell lines, ruxolitinib decreased pSTAT5 to basal levels and pERK to a lesser extent. Umbralisib reduced pAKT and pS6, but neither pERK nor pSTAT5 was significantly affected. The combination again was unique in its ability to reduce all four signaling molecules to near-basal levels. Experimental replicates with their corresponding dotplots and each cell line's response to GM-CSF stimulation can be found in the Supplementary Figure E2 (online only, available at www.exphem.org).

Given the pattern of PI3K catalytic subunit expression observed in cells with a monocytic histological phenotype,

Table 1. CMML patient characteristics and response to individual agents

Pt ID	Symbol	GENDER	Age at Dx	WHO Category	Blast% BMBx	Karyotype at Diagnosis	Molecular Abberations	GI50 Ruxolitinib (μM)	GI50 Umbralisib (μM)
CMML 001	▼	M	67	CMML-1	2.5	46XY	ASXL1, EZH2, TET2	0.095	11.87
CMML 002	♦	F	67	CMML-2	10.0	46XX del(9) (q13,q32)	RUNX1, SRSF2	0.021	2.257
CMML 003	⬢	M	62	CMML-2	10.0	45XY	ASXL1, IDH2, SRSF2	67.067	>100
CMML 004	○	F	63	CMML-1	5.0	46XX del(7) (q22,q32)	JAK2	2.39	0.354
CMML 005	●	M	72	CMML-1	9.5	46XY	ASXL1, RUNX1	0.549	18.2
CMML 006	×	F	66	CMML-1	7.0	46XX	ASXL1, NRAS, ETV6, SRSF2, SETBP1	0.549	>100
CMML 007	■	M	65	CMML-2	17.5	46XY	ASXL1, EZH2, RUNX1, IDH2, PHF6	0.126	5.969
CMML 008	□	M	74	CMML-1	5.0	46XY	None detected	0.509	14.10861999
CMML 009	+	M	59	CMML-1	5.0	46XY	ASXL1, RUNX1, JAK2, IDH2, SRSF2	0.102	2.289
CMML 010	▽	M	73	CMML-2	12.0	46XY t(6;13) (p23,q14)	ASXL1, NRAS, SETBP1, GATA2	0.291	56.176
CMML 011	▲	F	76	CMML-1	0.8	46XX	DNMT3A, SF3B1, TET2	0.002	8.136
CMML 012	★	M	66	CMML-1	<5%	45XY	ASXL1, TET2, EZH2	58.092	>100
CMML 013	*	F	65	CMML-0	2.0	46XX	KRAS, TET2, SRSF2	NA	NA
CMML 014	△	F	57	CMML-1	10.0	46XX inv(2) (p11.2q13)	ASXL1, FLT3-ITD, SETBP1	NA	NA

*Clinical information corresponding to CMML patient samples. Karyotype and blast% values are from the time of diagnostic bone marrow biopsy. Samples were tested with targeted next-generation sequencing of 37 myeloid genes. Viably frozen CMML BMMNCs were treated ex vivo with threefold dilutions of ruxolitinib and umbralisib, and the GI50 at 72 hours was calculated.

we moved to study the activity of umbralisib in CMML patient samples, both as a solo agent and in combination with another emerging therapy, ruxolitinib. All studies were conducted on viably frozen BMMNCs from 14 CMML patients, with a diverse range of BM blast percentage and molecular aberrations as detected by a next-generation sequencing panel (Table 1; Supplementary Figure E3, online only, available at www.exphem.org). Congruent with previous reports, ruxolitinib effectively repressed growth of CMML samples in vitro, with a majority of samples having GI_{50} values between 2 and 550 nmol/L (Table 1) [2]. Umbralisib exhibited comparable efficacy in CMML patient samples as was shown in the MV-4-11 cell line, with a majority of GI_{50} values between 0.3 and 14 μmol/L (Table 1). Umbralisib had previously been reported to induce no cytotoxicity in healthy hematopoietic progenitor cells at concentrations >10 μmol/L, which is also a clinically achievable plasma concentration in humans treated with umbralisib [11,23].

CMML samples contained significant amounts of the PI3K-δ isoform protein as examined by Western blot (Figure 3A). The combination of 100 nmol/L ruxolitinib and 10 μmol/L umbralisib decreased viability in most samples tested beyond the monotherapy treatments and resulted in ZIP synergy scores ranging from 5 to 17, indicating an additive to synergistic effect, in a majority of patients tested (Figure 3B,C; Supplementary Figure E4, online only, available at www.exphem.org). The strongest synergy was found in the CMML samples 004, 006, and 009. All three harbor mutations in progrowth signaling pathways, including the only two samples with JAK2 mutations and a third containing a NRAS mutation. CFU assays further illustrated the ability of ruxolitinib + umbralisib to reduce clonogenicity to a greater extent than either agent alone (Figure 3D). Finally, the combination also decreased the viability, defined using flow cytometry as Annexin V^-/$DAPI^-$ cells of myeloid $CD33^+$/$CD45^+$ and hematopoietic stem cell $CD34^+CD38^-$ cell subpopulations (Figure 3E,F). Representative dotplots and gating strategy for these experiments can be found in the Supplementary Figure E5 (online only, available at www.exphem.org).

As was done with cell lines described above, a small number of available samples were subsequently investigated for cell signaling changes. As previously reported, ruxolitinib alone decreased pSTAT5 levels across three samples tested in response to stimulation with GM-CSF (Figure 3G). Assessment of pAKT signaling was limited by a weak response of this signaling pathway to GM-CSF stimulation in our patient samples; however, umbralisib has previously been reported to dose-dependently inhibit AKT phosphorylation across a range of cell lines [24]. Solo agent treatment with umbralisib resulted in significant increases in pSTAT5 in two of three samples, consistent with studies describing STAT5-mediated resistance to solo agent PI3K-AKT pathway inhibition [7]. The combination treatment resulted in a unique pattern of signaling changes, including consistent pS6 and pERK downregulation, as was seen in both cell lines. Although not observed consistently across samples tested, a unique basal pERK signaling pattern was observed in a single NRAS-mutant sample in the absence of GM-CSF stimulation, CMML 010, which exhibited an increase in pERK in the presence of ruxolitinib alone but a decrease when combined with umbralisib, as was seen in the THP-1 cell line (Figure 3H).

Discussion

CMML is associated with significant morbidity and mortality and affects predominately patients of advanced age, limiting the utility of HSCT. Current treatment options centered around hydroxyurea and DNA methyltransferase inhibitors (DNMTi) do not significantly alter the natural disease course in most

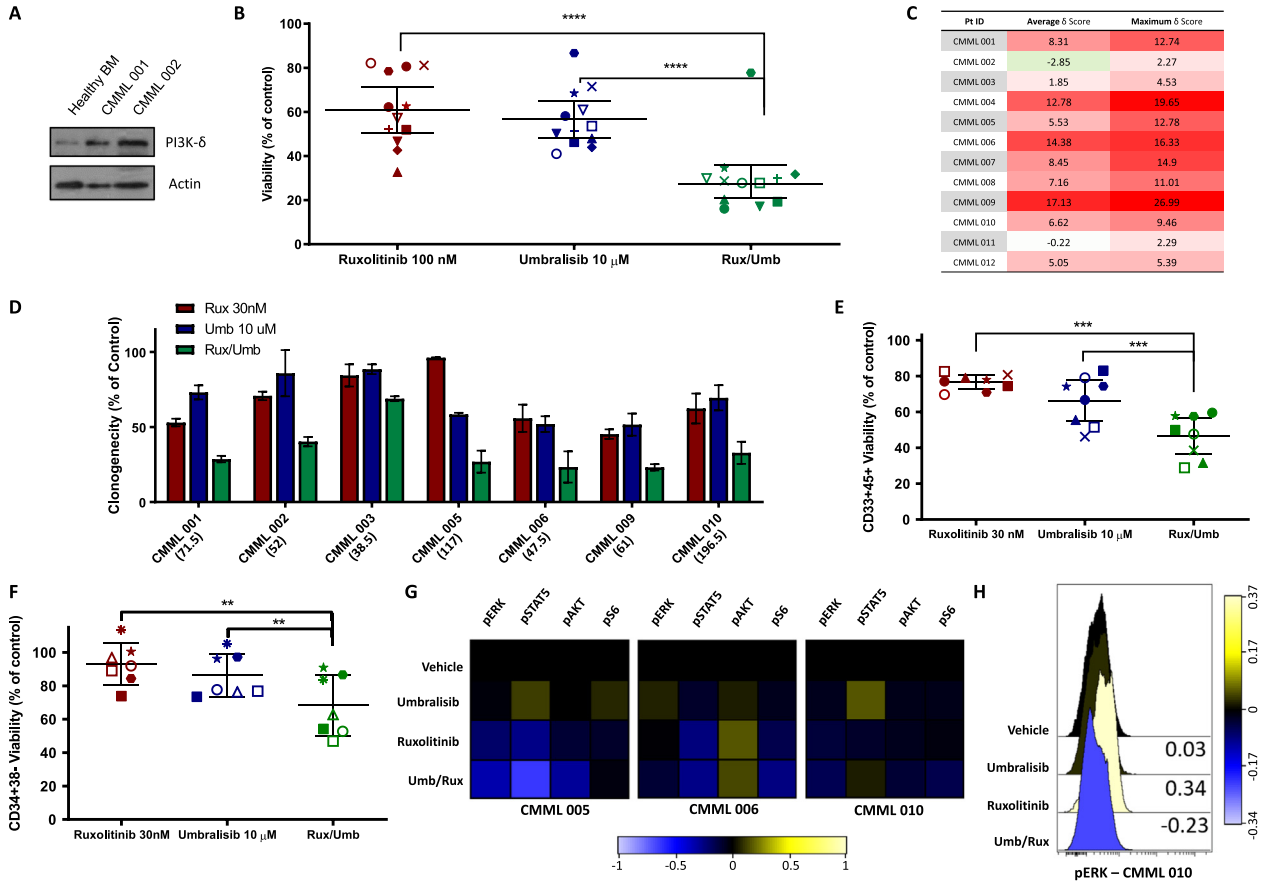

Figure 3. Ruxolitinib/umbralisib combination ex vivo treatment of CMML patient samples. **(A)** Western blot analysis of two CMML patient bone marrow samples and 1 healthy bone marrow sample. Actin was used as a loading control. **(B)** The viability of treated cells compared with that of the DMSO control using the CellTiter-Glo assay was plotted for the indicated concentrations. Individual patients are represented by specific shapes (two-tailed *t* test; *n.s.*=not significant, $*p < 0.05$, $**p < 0.01$, $***p < 0.005$, $****p < 0.001$). **(C)** The overall ZIP δ synergy score was based on the entire range of doses tested, and the most synergistic area score was based on the specific concentrations that had the highest synergy for each CMML sample tested. *Red shading* indicates increasing synergy values. (**D**) Inhibitory effect of ruxolitinib (Rux), umbralisib (Umb), and the combination (Rux/Umb) on CFU-GM growth from CMML samples stimulated with GM-CSF. Colony growth was assessed after 14 days. Results are expressed as the percentage CFU-GM growth relative to cultures without drug. Multiple regression analysis confirmed that the combination treatment reduced clonogenicity more than either individual drug treatment ($p < 0.001$). Numbers in parentheses below horizontal labels represent the average number of colonies counted in each experiment with respect to the control condition. (**E,F**) Viability was determined by annexin V/DAPI staining using flow cytometry with viable cell defined as $AnnexinV^{-}DAPI^{-}$ for both early myeloid ($CD45^{+}/CD33^{+}$) at 24 hours and hematopoietic stem cells ($CD34^{+}CD38^{-}$) at 48 hours. Each symbol represents a single experimental replicate for each patient sample. (**G**) Heatmap revealing phosphorylated signaling protein changes measured using phospho-specific flow cytometry. Samples were incubated with DMSO, umbralisib, ruxolitinib, or the combination for 30 min and subsequently incubated with GM-CSF for 15 min before fixing and staining. Color shading represents arcsinh values of the median fold change from DMSO-treated cells. (**H**) Histograms of pERK protein levels under unstimulated culture conditions (without addition of GM-CSF) in response to ruxolitinib, umbralisib, or their combination in a single NRAS-mutant patient sample. Values represent the arcsinh of the median fold change from DMSO-treated cells.

patients [25,26]. Early clinical trial data have indicated that ruxolitinib may improve the inflammatory symptoms that burden CMML patients, but no evidence yet exists that ruxolitinib alone can improve survival in CMML [3]. Preclinical studies have identified complex hyperactivated signaling networks that sustain clonal growth of myeloid cells in the presence of ruxolitinib, suggesting that treatment with a combination of signal transduction inhibitors may be necessary to effectively treat the disease in some cases [25].

In this study, we have identified a pattern of PI3K catalytic subunit expression, namely, increased PI3*KCD* and decreased *PIK3CA*, which correlates with a monocytic histological phenotype, including both M5 AML and CMML. Although a mechanistic explanation for this gene expression pattern was not sought by this study, we propose a likely mechanism based on recently published CMML single-cell RNA sequencing data [27]. PI3K-δ is regulated primarily at the transcription level, and transcription factor (TF)

binding cluster analysis has identified a handful of key TFs that regulate *PIK3CD* expression, including IRF and NFAT family members [20]. IRF has recently been reported to be upregulated in CMML hematopoietic stem cells, and both IRF and NFAT TFs are known to play a key role in expression of monocyte-specific genes [27–29]. It is possible that the common phenotype of monocytic predominance shared by the otherwise heterogeneous disease of CMML is driven by a promonocytic differentiation and pro-inflammatory TF networks, and these same TFs preferentially promote the expression of *PIK3CD* over the other PI3K catalytic subunit genes.

Our investigation of primary CMML patient samples reveals a promising relationship between JAK1/2 inhibition and PI3K-δ inhibition. Studies of signaling protein changes offer a hypothesis based on the unique ability of this combination to prevent activation of the S6, STAT5, and ERK pathways simultaneously. ERK has previously been identified as a compensatory mechanism to JAK inhibitors in MPNs and has been reported to play a key role in the GM-CSF hypersensitivity observed in an oncogenic NRAS CMML model [30,31]. PI3K/AKT signaling has been found to regulate ERK activation in $JAK2^{V617F}$ mutant myelofibrosis patient samples, and notably, the two CMML samples we studied that harbored JAK2 mutations had the two highest synergy scores [32]. PI3K-δ, specifically, was necessary for GM-CSF–mediated ERK activation in a juvenile myelomonocytic leukemia model [33]. Although this pattern was observed, it was not consistent across our already limited number of patient samples. It is unsurprising a clear and consistent signaling pattern was not generated with CMML patient samples given the heterogeneity of this disease, and these signaling changes should not be expected to be observed across all CMML patients.

Among the PI3K subunit isoforms, the PI3K-δ protein has unique relevance for the treatment of bone marrow neoplasms [10]. PI3K-δ-targeting therapies have been frequently associated with autoimmune phenomena, which limit their tolerability, attributed to their suppressive effects on T regulatory cells, but this appears to be less true of umbralisib [9,34,35]. In this context, these preclinical data indicate novel synergistic activity in CMML by co-inhibition of PI3K-δ and JAK1/2 with two well-tolerated pharmaceuticals at clinically relevant doses and support the use of ruxolitinib/umbralisib combination therapy in CMML under active clinical investigation (NCT02493530).

Conflict of interest disclosure

MRS receives research funding from Astex, Incyte, Millennium, and TG Therapeutics; serves on consultancy/advisory board/monitoring committees for AbbVie, Astex, BMS, Celgene, Geron, Karyopharm, Millennium, Ryvu, Sunesis, and TG Therapeutics; has equity in Karyopharm; and has patents and royalties with Boehringer-Ingelheim. The remaining authors have no competing financial interests.

Acknowledgments

MRS is generously supported by the Biff Ruttenberg Foundation, the Aventure Alle Fund, the Beverly and George Rawlings Directorship, and is a Clinical Scholar for the Leukemia and Lymphoma Society. This work was also supported by the Vanderbilt-Ingram Cancer Center (NCI P30 CA 68485), and TG Therapeutics which provided umbralisib and other support for this work. The authors also thank Peter Sportelli and Hari Miskin of TG Therapeutics who provided key insight from ongoing clinical umbralisib studies. Patient samples were garnered from the Vanderbilt-Ingram Cancer Center (VICC) Hematologic Malignancy Tumor Bank. The REDCap database tool is supported by grant UL1 TR000445 from NCATS/NIH. Flow Cytometry experiments were performed in the VUMC Flow Cytometry Shared Resource. The VUMC Flow Cytometry Shared Resource is supported by the Vanderbilt-Ingram Cancer Center (P30 CA68485) and the Vanderbilt Digestive Disease Research Center (DK058404). The authors were aided by the Cancer Cell Line Encyclopedia, generously provided to the public by the Broad Institute.

References

1. Itzykson R, Kosmider O, Renneville A, et al. Prognostic score including gene mutations in chronic myelomonocytic leukemia. J Clin Oncol. 2013;31:2428–2436.
2. Padron E, Painter JS, Kunigal S, et al. GM-CSF-dependent pSTAT5 sensitivity is a feature with therapeutic potential in chronic myelomonocytic leukemia. Blood. 2013;121:5068–5077.
3. Padron E, Dezern A, Andrade-Campos M, et al. A multi-institution phase I trial of ruxolitinib in patients with chronic myelomonocytic leukemia (CMML). Clin Cancer Res. 2016;22:3746–3754.
4. Geissler K, Ohler L, Födinger M, et al. Interleukin 10 inhibits growth and granulocyte/macrophage colony-stimulating factor production in chronic myelomonocytic leukemia cells. J Exp Med. 1996;184:1377–1384.
5. Britschgi A, Andraos R, Brinkhaus H, et al. JAK2/STAT5 inhibition circumvents resistance to PI3K/mTOR blockade: a rationale for cotargeting these pathways in metastatic breast cancer. Cancer Cell. 2012;22:796–811.
6. Bartalucci N, Tozzi L, Bogani C, et al. Co-targeting the PI3K/mTOR and JAK2 signalling pathways produces synergistic activity against myeloproliferative neoplasms. J Cell Mol Med. 2013;17:1385–1396.
7. Choong ML, Pecquet C, Pendharkar V, et al. Combination treatment for myeloproliferative neoplasms using JAK and pan-class I PI3K inhibitors. J Cell Mol Med. 2013;17:1397–1409.
8. Kurtz SE, Eide CA, Kaempf A, et al. Molecularly targeted drug combinations demonstrate selective effectiveness for myeloid- and lymphoid-derived hematologic malignancies. Proc Natl Acad Sci USA. 2017;114:E7554–E7563.

9. Burris HA, Flinn IW, Patel MR, et al. Umbralisib, a novel PI3Kδ and casein kinase-1ε inhibitor, in relapsed or refractory chronic lymphocytic leukaemia and lymphoma: an open-label, phase 1, dose-escalation, first-in-human study. Lancet Oncol. 2018;19:486–496.
10. Sujobert P, Bardet V, Cornillet-Lefebvre P, et al. Essential role for the p110δ isoform in phosphoinositide 3-kinase activation and cell proliferation in acute myeloid leukemia. Blood. 2005;106:1063–1066.
11. Billottet C, Grandage VL, Gale RE, et al. A selective inhibitor of the p110δ isoform of PI 3-kinase inhibits AML cell proliferation and survival and increases the cytotoxic effects of VP16. Oncogene. 2006;25:6648–6659.
12. Moyo TK, Palmer J, Huang Y, et al. Resurrecting response to ruxolitinib: a phase I study testing the combination of ruxolitinib and the PI3K delta inhibitor umbralisib in ruxolitinib-experienced myelofibrosis. Hemasphere. 2018;2:19–20.
13. Pölönen P, Mehtonen J, Lin J, et al. HEMap: an interactive online resource for characterizing molecular phenotypes across hematologic malignancies. Cancer Res. 2019;79:2466–2479.
14. Barretina J, Caponigro G, Stransky N, et al. The Cancer Cell Line Encyclopedia enables predictive modelling of anticancer drug sensitivity. Nature. 2012;483:603–607.
15. Babicki S, Arndt D, Marcu A, et al. Heatmapper: web-enabled heat mapping for all. Nucleic Acids Res. 2016;44:W147–W153.
16. Yadav B, Wennerberg K, Aittokallio T, Tang J. Searching for drug synergy in complex dose–response landscapes using an interaction potency model. Comput Struct Biotechnol J. 2015;13:504–513.
17. Irish JM, Kotecha N, Nolan GP. Mapping normal and cancer cell signalling networks: towards single-cell proteomics. Nat Rev Cancer. 2006;6:146–155.
18. Earl DC, Ferrell PB, Leelatian N, et al. Discovery of human cell selective effector molecules using single cell multiplexed activity metabolomics. Nat Commun. 2018;9:1–12.
19. Krutzik PO, Nolan GP. Fluorescent cell barcoding in flow cytometry allows high-throughput drug screening and signaling profiling. Nat Methods. 2006;3:361–368.
20. Kok K, Nock GE, Verrall EAG, et al. Regulation of p110δ PI 3-kinase gene expression. PLoS One. 2009;4:e5145.
21. Gelsi-Boyer V, Cervera N, Bertucci F, et al. Gene expression profiling separates chronic myelomonocytic leukemia in two molecular subtypes. Leukemia. 2007;21:2359–2362.
22. Iyengar S, Clear A, Maharaj L, et al. P110a-mediated constitutive PI3K signaling limits the efficacy of p110d-selective inhibition in mantle cell lymphoma, particularly with multiple relapse. Blood. 2013;121:2274–2284.
23. Locatelli SL, Careddu G, Inghirami G, et al. The novel PI3K-δ inhibitor TGR-1202 enhances brentuximab vedotin-induced Hodgkin lymphoma cell death via mitotic arrest. Leukemia. 2016;30:2402–2405.
24. Deng C, Lipstein MR, Scotto L, et al. Silencing c-Myc translation as a therapeutic strategy through targeting PI3Kδ and CK1ε in hematological malignancies. Blood. 2017;129:88–99.
25. Moyo TK, Savona MR. Therapy for chronic myelomonocytic leukemia in a new era. Curr Hematol Malig Rep. 2017;12:468–477.
26. Merlevede J, Droin N, Qin T, et al. Mutation allele burden remains unchanged in chronic myelomonocytic leukaemia responding to hypomethylating agents. Nat Commun. 2016;7:10767.
27. Wiseman DH, Baker SM, Dongre AV, et al. Chronic myelomonocytic leukaemia stem cell transcriptomes anticipate disease morphology and outcome. EBioMedicine. 2020;58:102904.
28. Ozato K, Tailor P, Kubota T. The interferon regulatory factor family in host defense: mechanism of action. J Biol Chem. 2007;282:20065–20069.
29. Rao A. NF-ATp: a transcription factor required for the co-ordinate induction of several cytokine genes. Immunol Today. 1994;15:274–281.
30. Wang J, Liu Y, Li Z, et al. Endogenous oncogenic NRAS mutation promotes aberrant GM-CSF signaling in granulocytic/monocytic precursors in a murine model of chronic myelomonocytic leukemia. Blood. 2010;116:5991–6002.
31. Stivala S, Codilupi T, Brkic S, et al. Targeting compensatory MEK/ERK activation increases JAK inhibitor efficacy in myeloproliferative neoplasms. J Clin Invest. 2019;129:1596–1611.
32. Wolf A, Eulenfeld R, Gäbler K, et al. JAK2-V617F-induced MAPK activity is regulated by PI3K and acts synergistically with PI3K on the proliferation of JAK2-V617F-positive cells. JAK-STAT. 2013;2:e24574.
33. Goodwin CB, Li XJ, Mali RS, et al. PI3K p110δ uniquely promotes gain-of-function Shp2-induced GM-CSF hypersensitivity in a model of JMML. Blood. 2014;123:2838–2842.
34. Chellappa S, Kushekhar K, Munthe LA, et al. The PI3K p110δ isoform inhibitor idelalisib preferentially inhibits human regulatory T cell function. J Immunol. 2019;202:1397–1405.
34. Maharaj K, Powers JJ, Achille A, et al. The dual PI3Kδ/CK1ε inhibitor umbralisib exhibits unique immunomodulatory effects on CLL T cells. Blood Adv. 2020;4:3072–3084.

Supplementary Methods

Drug combination analysis and calculation of synergy. To assess the efficacy of the combination of umbralisib and ruxolitinib compounds, cells were plated and viability determined as described above using 3-fold dilution matrices of umbralisib and ruxolitinib. The effects of the combinations were calculated using the Zero Interaction Potency (ZIP) model, which compares observed and expected combination effects.[1] The ZIP model combines the advantages of the Bliss independence and Loewe additivity models. As a null hypothesis, it assumes that two non-interacting drugs will incur minimal changes in their drug response curve. The output of the ZIP model is the delta synergy score (δ), which is the average combination effect of the drugs over the total dose matrix tested. The synergy scores can be interpreted as the average excess response due to drug interactions (i.e. a delta score of 10 corresponds to 10% of response beyond expectation). There is no delta score threshold to define a combination as synergistic. However, based on the

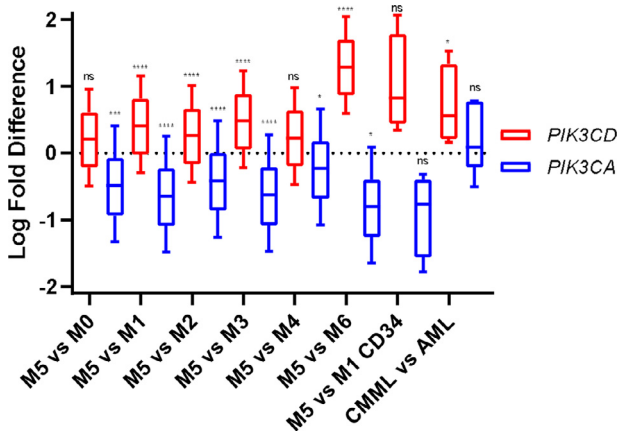

Figure S1. PIK3CA and PIK3CD gene expression comparisons by leukemia type. Box and whisker plots representing mean log fold difference between two myeloid disease subsets derived from Affymetrix Human Genome U133 Plus 2.0 Array probe sets. Data is the same as that presented in Figure 1D. Benjamini-Hochberg Adjusted p-value; n.s. not significant, *p < 0.05, **p <0 .01, ***p<0.005, ****p<0.001. AML data is derived from the Hemap database. CMML data are derived from Gelsi-boyer et al.

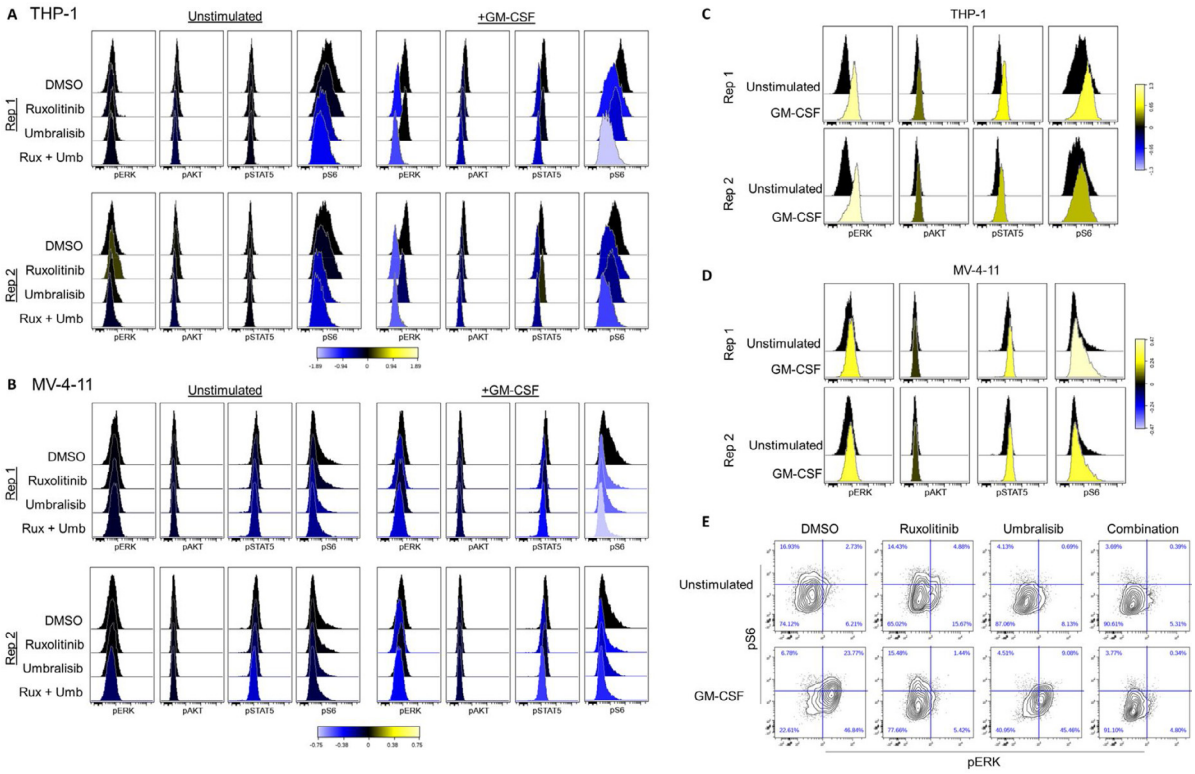

Figure S2. Cell signaling pathways in myeloid leukemia cell lines in response to ruxolitinib/umbralisib. (A-B) Histograms representing complete data from phospho-specific flow cytometry experiments with THP-1 and MV-4-11 cell lines in both the presence and absence of GM-CSF stimulation demonstrating the effect of ruxolitinib, umbralisib and their combination on cell signaling. (C-D) Histograms demonstrating the cell-signaling response to GM-CSF stimulation of two cell lines. (E) Contour plots depicting the ratio of pERK, pS6 and double positive staining THP-1 cells when exposed to the single agents or drug combination.

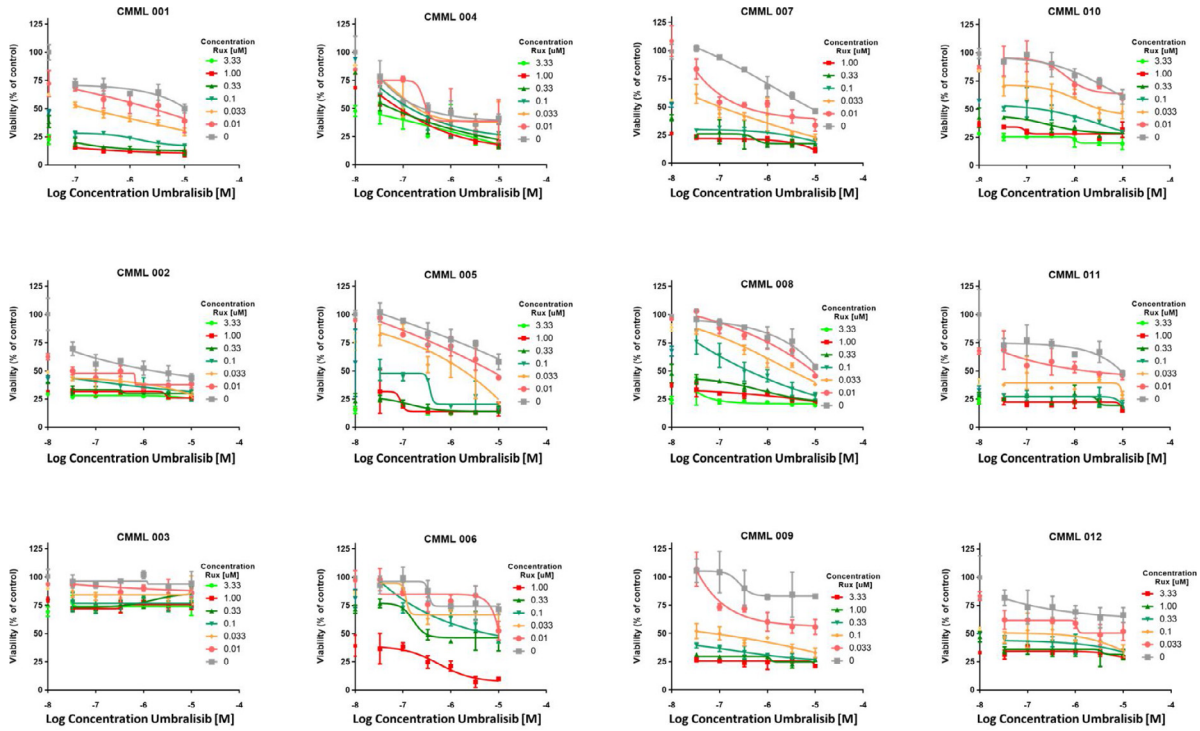

Figure S3. CMML patient samples display differential responses to combination JAK1/2 and PI3K-δ inhibition. CMML BMMNCs were treated ex vivo with three-fold dilutions of ruxolitinib (Rux), umbralisib (Umb) or a combination (Rux/Umb) for 72 hours to generate dose response curves.

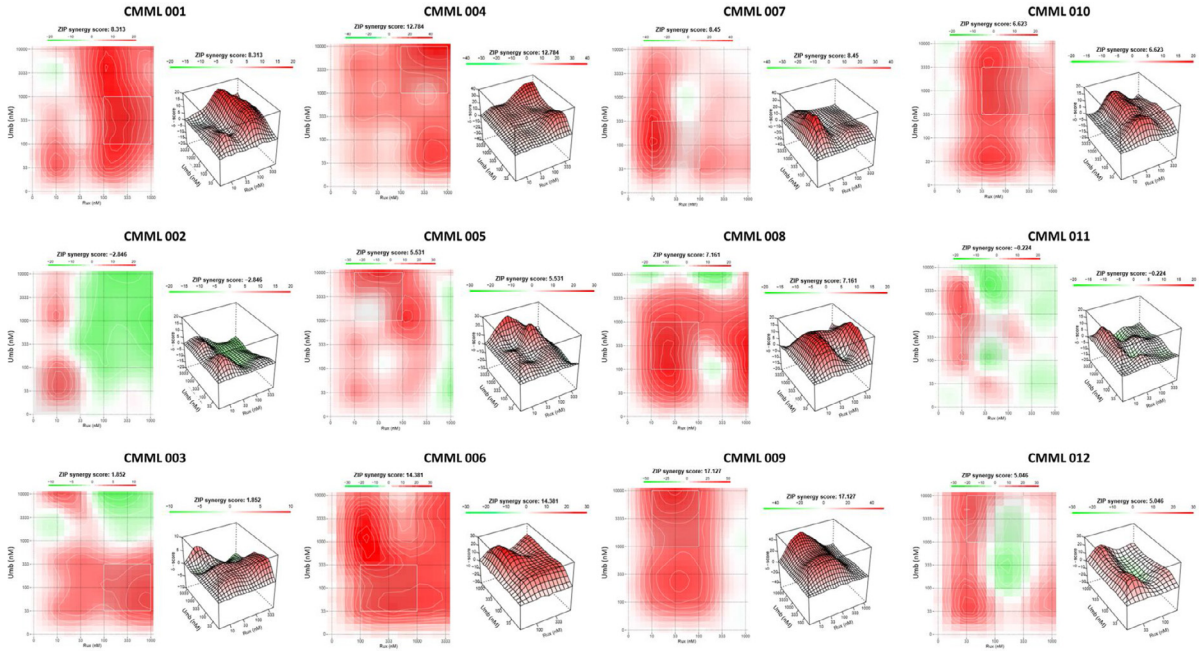

Figure S4. CMML patient samples display differential synergy to combination JAK1/2 and PI3K-δ inhibition. Contour plots of synergy scores generated from a dose matrix of Rux/Umb using the ZIP model. The synergy scores were represented by pseudocoloring 2-D (left panel) or 3-D (right panel) contour plots over the dose matrix, giving rise to the overall synergy landscape. Red color indicates synergy, while green color indicates antagonism for the various concentrations of the Rux/Umb combination. Note different scale bars for ZIP synergy scores for each patient sample.

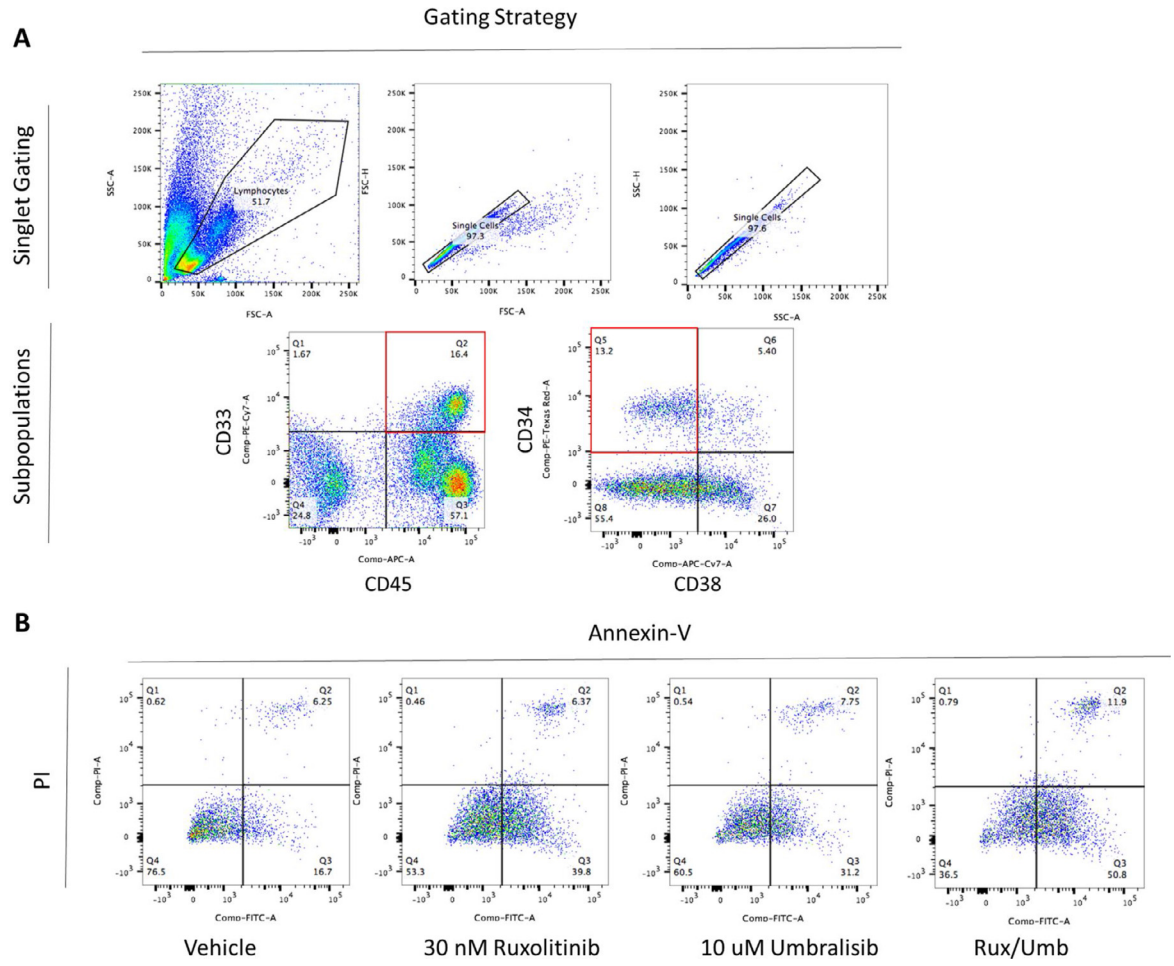

Figure S5. Representative gating strategy for assessment of viability in myeloid subpopulations. (A) Representative dot plots and gating strategy used to define both early myeloid ($CD45^+/CD33^+$) and hematopoietic stem cells ($CD34^+/CD38^-$) from CMML patient sample CMML 004. (B) Representative dot plots and gating strategy to determine viable cells ($AnnexinV^-DAPI^-$) within the $CD45^+/CD33^+$ subpopulation of the patient sample CMML 004.

Table S1. Differential PI3K catalytic subunit gene expression values and P-values by disease type. The log2 fold difference, two-tailed Wilcoxon test followed by Benjamini-Hochberg adjustment of P-values (adj.P-value) were computed to compare gene expression levels for *PIK3CA, PIK3CB, PIK3CD, PIK3CG* across the indicated disease subtypes.

Comparison	Gene	P-Value	Log Fold Change	adj.P-Value	Data Source
M0 vs M5	*PIK3CD*	5.48E-02	-0.217	2.12E-01	GSE6891
M1 vs M5	*PIK3CD*	7.27E-14	-0.663	2.74E-12	GSE6891
M2 vs M5	*PIK3CD*	3.07E-07	-0.383	4.23E-06	GSE6891
M3 vs M5	*PIK3CD*	6.75E-04	-0.315	4.31E-03	GSE6891
M4 vs M5	*PIK3CD*	1.50E-02	-0.194	2.48E-01	GSE6891
M6 vs M5	*PIK3CD*	5.02E-10	-1.600	3.61E-08	GSE6891
M1 vs M5 CD34	*PIK3CD*	1.01E-01	-1.270	3.98E-01	GSE12326
AML vs CMML	*PIK3CD*	4.23E-03	-0.701	4.71E-02	GSE42731
AML vs CMML	*PIK3CD*	5.52E-03	-0.676	8.08E-02	GSE61804
M0 vs M5	*PIK3CA*	6.40E-05	0.324	1.68E-03	GSE6891
M1 vs M5	*PIK3CA*	5.26E-15	0.550	2.47E-13	GSE6891
M2 vs M5	*PIK3CA*	1.00E-17	0.621	2.04E-15	GSE6891
M3 vs M5	*PIK3CA*	1.36E-08	0.680	2.99E-07	GSE6891
M4 vs M5	*PIK3CA*	9.43E-04	0.228	4.62E-02	GSE6891
M6 vs M5	*PIK3CA*	1.76E-03	0.495	1.32E-02	GSE6891
AML vs CMML	*PIK3CA*	7.58E-02	0.427	3.07E-01	GSE42731
AML vs CMML	*PIK3CA*	1.25E-01	0.380	4.18E-01	GSE61804
M1 vs M5 CD34	*PIK3CA*	2.72E-02	1.600	2.51E-01	GSE12326

Table S2. Mean gene expression values of PI3K catalytic subunits. Values represent mean log2-transformed expression values of Affymetrix Human Genome U133 Plus 2.0 Array probe sets. AML, MDS and CML data are derived from the Hemap database. CMML data are derived from Gelsi-boyer et al.

NAME	PIK3CA	PIK3CB	PIK3CD	PIK3CG
M0 (n = 67)	7.225	6.568	7.279	6.399
M1 (n = 131)	7.397	7.346	7.049	5.889
M2 (n = 205)	7.323	7.43	7.196	6.178
M3 (n = 71)	7.364	8.06	7.022	5.877
M4 (n = 160)	7.073	7.323	7.235	6.304
M5 (n = 100)	6.832	7.559	7.499	6.627
M6 (n = 26)	7.495	7.954	6.511	5.587
Monocytes (n = 25)	7.578	7.394	7.988	6.534
Healthy CD34 (n = 21)	7.236	7.114	6.942	6.206
AML CD34 (n = 58)	7.149	7.689	6.938	6.162
M1 CD34 (n = 2)	7.096	6.531	7.015	5.371
M5 CD34 (n = 4)	6.309	6.672	7.849	5.844
MDS (n = 423)	7.051	7.416	6.984	5.957
CML (n = 274)	7.199	7.567	6.667	5.824
CMML (n = 11)	8.004	7.980	10.011	7.458

Table S3. Clinical information for CMML patient samples. Karyotype and complete blood count (CBC) values are from the time of diagnostic bone marrow biopsy. Hgb = hemoglobin (x 10^3), WBC = white blood cells (x 10^3), platelets (x 10^3), monocytes = absolute monocytes. Splenomegaly was considered positive if it was documented in the patient's electronic medical record (EMR) during initial clinic visit with oncologist.

Sample ID	Age at Dx	GENDER	HgB at Dx	WBC at Dx	platelets at Dx	Splenomegaly
CMML 001	67	M	13.2	41.5	120	-
CMML 002	67	F	9.7	4.7	71	-
CMML 003	62	M	12.1	2.6	55	-
CMML 004	60	F	10.9	7.9	863	+
CMML 005	72	M	9.8	4.2	198	-
CMML 006	66	F	9.5	67.7	176	-
CMML 007	65	M	11.6	19.4	9	-
CMML 008	74	M	8.6	8.2	277	-
CMML 009	59	M	11.9	13.9	51	-
CMML 010	56	M	12.5	14.9	86	+
CMML 011	76	F	6.0	6.5	354	+
CMML 012	66	M	12.1	38.5	109	-
CMML 013	65	F	12.0	45.0	311	-
CMML 014	57	F	7.7	18.4	99	+

Table S4. Clinical NGS panel results for patient samples; (-), not detected; NA, not available, (+) disease-associated mutation detected in gene without details of molecular aberration. Samples were tested with the OnkoSight™ NGS Myeloid Malignancies gene panel unless otherwise specified; other genes tested with this panel that were not detected in any of the samples include ABL1, BCOR, BCORL1, BRAF, CALR, CBL, CDKN2A, FBXW7, FLT3-TKD, HRAS, IDH1, KIT, MPL, MYD88, NPM1, U2AF1, WT1, ZRSR2.

Sample ID	ASXL1	FLT3-ITD	EZH2	DNMT3A	NPM1	TET2	TP53	SF3B1	RUNX1	NRAS	KRAS	JAK2	IDH1	IDH2	CBL	CDNK2A	ETV6	GATA2	PTPN11	SRSF2	U2AF1	PHF6	PTEN	SETBP1
CMML 001	p.Glu635Argfs*15/p.Gly949Val	-	p.Asp142Val	-	p.Phe1287Leufs*76/ p.Gly1861Glufs*26	-	-	-	-	-	-	-	-	-	-	-	-	-	-	-	-	-	-	-
CMML 002	-	-	-	-	-	-	-	p.Thr111_Lys117del	-	-	-	-	-	-	-	-	-	-	-	p.Pro95His	-	-	-	-
CMML 003	p.Tyr700Leufs*18	-	-	-	-	-	-	-	-	-	-	-	-	p.Arg172Lys	-	-	-	-	-	p.Pro95Arg	-	-	-	-
CMML 004*	NA	NA	NA	NA	NA	NA	NA	NA	NA	NA	NA	p.Val617Phe	NA	NA	NA	NA	NA	NA	NA	NA	NA	NA	NA	NA
CMML 005	p.Glu635Argfs*15	-	-	-	-	-	-	-	p.Phe336Profs*265	-	-	-	-	-	-	-	-	-	-	-	-	-	-	-
CMML 006	p.Cys789Metfs*2	-	-	-	-	-	-	-	-	p.Gly12Ser	-	-	-	-	-	-	p.Arg353Pro	-	-	p.Pro95His	-	-	-	p.Asp868Asn
CMML 007	p.Glu635Argfs*15	-	p.Arg658Gly	-	-	-	-	-	p.Gln397Alafs*2-3	-	-	-	-	p.Arg140Gln	-	-	-	-	-	-	-	p.Arg225*	-	-
CMML 008	-	-	-	-	-	-	-	-	-	-	-	-	-	-	-	-	-	-	-	-	-	-	-	-
CMML 009	p.Glu635Argfs*15	-	-	-	-	-	-	-	p.Arg166*	-	-	p.Val617Phe	-	p.Arg140Gln	-	-	-	+	-	p.Arg944dup	-	-	-	-
CMML 010	+	-	-	-	-	-	-	-	-	+	-	-	-	-	-	-	-	-	-	-	-	-	-	+
CMML 011	-	-	-	-	+	-	+	-	-	-	-	-	-	-	-	-	-	-	-	-	-	-	-	-
CMML 012	+	-	+	-	+	-	-	-	-	-	-	-	-	-	-	-	-	-	-	-	-	-	-	-
CMML 013	-	-	-	-	+	-	-	-	-	-	+	-	-	-	-	-	-	-	-	+	-	-	-	-
CMML 014	p.Thr936Profs*9	p.				Pro606_Phe612dup	-	-	-	-	-	-	-	-	-	-	-	-	-	-	-	-	-	-
-	-	-	p.			Asp868Asn																		

experience of the creators of the ZIP synergy model, delta scores can be interpreted as follows:

- Less than -10: the interaction between two drugs is likely to be ***antagonistic***;
- From -10 to 10: the interaction between two drugs is likely to be ***additive***;
- Larger than 10: the interaction between two drugs is likely to be ***synergistic***.[2]

References

1. Yadav B, Wennerberg K, Aittokallio T, et al. Searching for Drug Synergy in Complex Dose–Response Landscapes Using an Interaction Potency Model. *Comput Struct Biotechnol J*. 2015, 13, 504-513.
2. Ianevski A, Giri AK, Aittokallio T. SynergyFinder 2.0: visual analytics of multi-drug combination synergies. *Nucleic Acids Res*. 2020,(1).